OPEN ACCESS
JOURNAL OF ADVANCED DIELECTRICS
Vol. 11, No. 6 (2021) 2150027 (7 pages)

DOI: 10.1142/S2010135X21500272

Dielectric relaxation and scaling of AC conductivity observed in mixed valence perovskite Eu_2CoMnO_6

Md. G. Masud[*,§] and B. K. Chaudhuri[†,‡]

[*]*Department of Physics, Basanti Devi College, 147B Rash Behari Avenue, Kolkata 700 029, India*

[†]*Center for Rural and Cryogenic Technologies, Jadavpur University, Kolkata 700 032, India*

[‡]*Formerly at Solid State Physics Department, Indian Association for the Cultivation of Science Kolkata 700 032, India*

[§]physics.masud@gmail.com

Received 16 August 2021; Accepted 26 October 2021; Published 20 November 2021

Monophasic and polycrystalline double perovskite Eu_2CoMnO_6 has been synthesized, and its structural characterization, frequency and temperature-dependent dielectric relaxation have been studied. Observed thermally activated dielectric relaxation was explained using the empirical Havriliak–Negami (HN) dielectric relaxation function with an estimated activation energy $E \sim 0.22$ eV and attempt frequency $f_0 \sim 2.46 \times 10^9$ Hz. The frequency-dependent AC conductivity data, over a wide range of temperature (100–325 K), followed the empirical universal power law behavior ($\sim f^n$, n is the constant exponent) showing two different frequency exponents, respectively, in the high- and low-temperature regions. The high-temperature (>275 K) conductivity data followed the continuous time random walk (CTRW) approximation model proposed by Dyre. However, this model failed to reproduce the observed conductivity spectra in the low-temperature side (<200 K). Interestingly, both the high- and low-temperatures' conductivity data can be scaled to the master curve with suitably chosen scaling parameters.

Keywords: Dielectric relaxation; AC conductivity; scaling; perovskite.

1. Introduction

Ferromagnetic insulators showing remarkable physical properties have drawn considerable research interest in recent years.[1–3] In this group, double perovskite is an exciting class of ferromagnetic insulators having the general chemical composition $A_2BB'O_6$ (A is lanthanum or rare earth, B/B' are two different transition metals and O is oxygen).[4–19] These multifunctional materials showed exciting multiferroic, magneto-dielectric and magneto-resistance properties having immense potential for their applications.[6–9] La_2CoMnO_6 and La_2NiMnO_6 are isostructural compounds of this double perovskite family which showed ferromagnetism and magnetoelectric properties.[9–12] One of the unique features of these double perovskites is the creation of anti-site disorder or anti-phase boundaries during the preparation of the compounds. Anti-site disorder induced unusual dielectric and magnetic properties were reported in different double perovskite compounds.[10–14]

In the past, detailed structural, dielectric and magnetic properties of single phase Eu_2NiMnO_6 revealed ferromagnetism with low coercivity and high dielectric constant associated with magnetodielectric features.[17] Recently, it was found that Eu_2CoMnO_6 showed unusual magnetic properties, Hopkinson-like effect as well as the presence of volume spin-glass-like behavior.[18] Though magnetic field induced metamagnetic, magnetocaloric and pyrocurrent were reported in the recent past,[19] the dielectric and AC conductivity characteristics of Eu_2CoMnO_6 have not yet been thoroughly investigated. Since dielectric study provides additional information of conduction and magnetoelectric coupling for such compounds,[9,10,20] our plan in this communication is to present detailed structural, dielectric and AC conductivity properties of Eu_2CoMnO_6 over broad ranges of temperature (80–350 K) and frequency (1 kHz–1 MHz). The observed temperature- and frequency-dependent dielectric properties of Eu_2CoMnO_6 indicated quite a high value of relative dielectric permittivity ~10^3 in the kHz frequency region. Thermally activated Havriliak–Negami (HN) type asymmetric and broadened dielectric relaxation was also noticed. CTRW and empirical universal dielectric response (UDR) analysis of the AC conductivity data have also been explored. These conductivity data exhibited interesting time-temperature scaling behavior as shown in this paper.

2. Material and Methods

Polycrystalline Eu_2CoMnO_6 was prepared by the standard solid state reaction route from a stoichiometric mixture of high purity (>99%) precursor EuO, CoO and MnO_2 oxides. The oxide precursors were well mixed using an agate mortar and then calcined at ~1000 K for 24 h. After grinding the calcined powder, pellets of diameter ~8 mm and ~2 mm

[§]Corresponding author.

thickness were made and sintered again at ~1200 K for 48 h and the furnace was cooled to ambient temperature. The crystalline structure of the sample was investigated by X-ray powder diffraction (using XRD-Bruker D8 Advance) with Cu-Kα radiation at ambient temperature and pressure. Dielectric permittivity and AC conductivity measurements were carried out using a HP 4192A impedance analyzer which was interfaced with a computer for automatic data acquisition. A good quality silver paste was used for the electrodes in the dielectric measurements. A Lakeshore 332 temperature controller was employed to control the sample temperatures with an accuracy of ~0.01 K. The refinement of the crystal structure was performed by the Rietveld method using the Material Analysis Using Diffraction (MAUD) program.

3. Results and Discussion

3.1. *Structural properties*

The crystallinity of the Eu_2CoMnO_6 compound was investigated from the analysis of the X-ray powder diffraction (XRD) as shown in Fig. 1. Monophasic and well crystalline nature of the prepared compound is evident from the observed sharp reflection lines. The X-ray diffraction patterns can be well fitted to the monoclinic space group $P2_1/n$. Based on the refinement result, a model crystal structure is developed and is shown in the inset of Fig. 1. The least square Rietveld refinement provides an estimate of lattice parameters $a = 5.333$, $b = 5.565$, $c = 7582$, $\alpha = 90.0°$, $\beta = 89.99°$ and $\gamma = 90°$. Goodness of the fit indicators associated with the refinement was $R_{wp} = 4.6$, $R_p = 3.58$ and $\sigma = 1.09$. The derived crystallographic parameters based on the refinement results are presented in

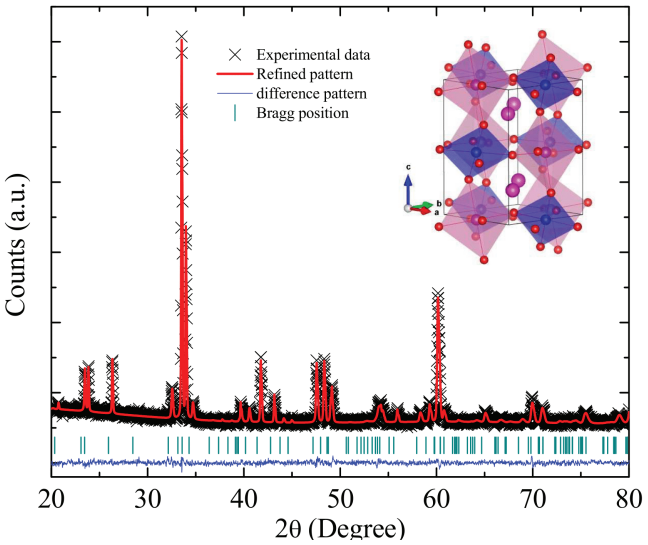

Fig. 1. (Color online) Powder X-ray diffraction pattern at room temperature. Red solid line is the least square Rietveld refinement of the XRD. The difference of observed and fitting result is shown by the blue continuous line. Green vertical ticks are Bragg positions for reflection lines.

Table 1. Comparison of structural information of Eu_2CoMnO_6 and isostructural Eu_2NiMnO_6. The data for Eu_2NiMnO_6 are taken from Ref. 17.

Structural parameters	Eu_2CoMnO_6	Eu_2NiMnO_6
a (Å)	5.334	5.332
b (Å)	5.565	5.523
c (Å)	7.582	7.595
Unit Cell Volume (Å^3)	225.06	223.66
<Co–O>(Å)	1.858	—
<Ni–O>(Å)	—	1.988
<Mn–O>(Å)	2.106	1.989
Mn–O1–Co/ Mn–O1–Ni	150.3°	144.5°
Mn–O2–Co/ Mn–O2–Ni	153.3°	141.7°
Mn–O3–Co/ Mn–O3–Ni	147.3°	163.3°
NiO_6 polyhedral volume	—	9.8726 (Å^3)
CoO_6 polyhedral volume	8.3785 (Å^3)	—
MnO_6 polyhedral volume	10.3325 (Å^3)	12.3008 (Å^3)

Table 1. A comparison of the Eu_2CoMnO_6 structure with the previously reported[17] isostructural and closely related double perovskite Eu_2NiMnO_6 is made and shown in a separate column in Table 1. The TM–O (TM = Ni, Mn, Co) bond distances are reduced for Co–O and enhanced for Mn–O when compared to Ni–O and Mn–O bond lengths observed in Eu_2NiMnO_6. In comparison to Eu_2NiMnO_6, the unit cell volume is slightly expanded; appreciable distortion and volume changes in the CoO_6 and MnO_6 polyhedral are also noticed. Interestingly, in comparison to Eu_2NiMnO_6, a significant deviation of the linear 180° situation of TM–O–TM in the apical 'c' direction is observed for the Eu_2CoMnO_6 compound. However, with respect to Eu_2NiMnO_6, the TM–O–TM angle in the basal plane deviates less from 180° in Eu_2CoMnO_6.

3.2. *Dielectric relaxations*

The measured frequency and temperature dependent relative dielectric permittivity (ε_r) of the pellet sample is shown in Fig. 2(a). At low frequency (f), quite a high value of $\varepsilon_r \sim 10^3$ (at 1 kHz) is observed even at a temperature as low as 185 K. With increasing frequency, the dielectric permittivity relaxes to a lower static dielectric value ($\varepsilon_\infty \sim 15$). The typical dielectric relaxation behavior shown in Fig. 2(a) differs appreciably from that of the ideal Debye type dielectric relaxation.[21] As shown in Fig. 2(a), the dielectric relaxation behavior can be fitted to the Havriliak–Negami (HN) dielectric relaxation model[22] described by

$$\varepsilon_r = \varepsilon_\infty + \Delta\varepsilon\left(1+2(\omega\tau)^\beta\cos\left(\frac{\pi\beta}{2}\right)+(\omega\tau)^{2\beta}\right)^{-\frac{\gamma}{2}}\cos(\gamma\varphi), \quad (1)$$

where $\Delta\varepsilon$ = dielectric strength, ω = angular frequency, τ = HN relaxation time, β, and γ parameters represent the symmetric and asymmetric broadening of the relaxation, respectively, and

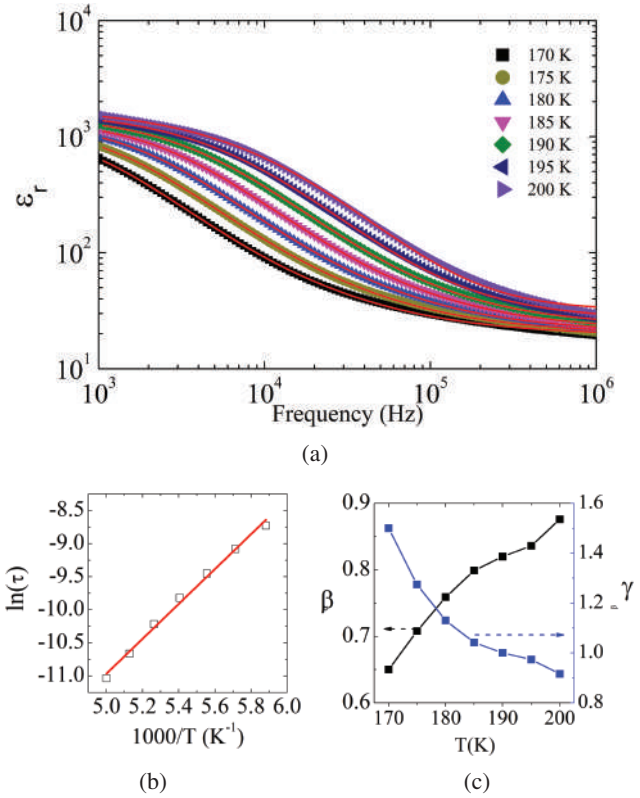

Fig. 2. (Color online) (a) Frequency variation of dielectric permittivity at some selected temperature. The solid red line is the best fit of HN relaxation function Eq. (1) discussed in text. (b) Arrhenius plot of the HN relaxation time; red line is best linear fit. (c) Temperature variation of asymmetric (β) and symmetric (γ) broadening parameters.

$$\varphi = \arctan\left(\frac{(\omega\tau)^{\beta}\sin\left(\frac{\pi\beta}{2}\right)}{1+(\omega\tau)^{\beta}\cos\left(\frac{\pi\beta}{2}\right)}\right).$$

It is seen from the red continuous line in Fig. 2(a) that the HN function replicated the observed dielectric relaxation quite reasonably. The temperature-dependent HN relaxation time τ obtained from the best fit to Eq. (1) is shown in Fig. 2(b) as a function of inverse temperature. An Arrhenius type thermally activated relaxation governed by $\tau = \tau_0 \exp\left(\frac{E}{kT}\right)$ (where τ_0 is the pre-exponential factor, E is the activation energy, k is the Boltzmann constant and T is the temperature) is found to follow. The best linear fit to the data provides a reasonable value of activation energy $E = 0.22$ eV and attempt frequency $f_0 = 2.46 \times 10^9$ Hz. Temperature variation of the asymmetry and broadness parameters obtained from the HN fitting to the dielectric relaxation is shown in Fig. 2(c). The symmetry parameter β increases with temperature and the asymmetry parameter γ decreases with temperature. Thus, different broadening mechanisms appeared to dominate at different temperatures.

The nonDebye type dielectric relaxation behavior is also evident from the modulus representation. The complex

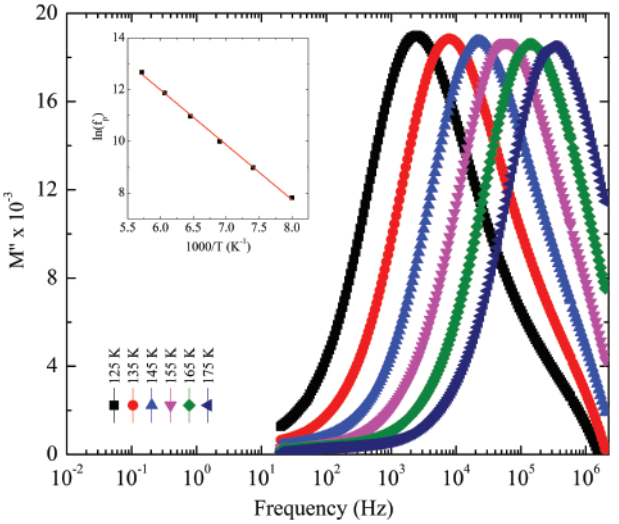

Fig. 3. (Color online) Thermally activated relaxation in the modulus representation. Inset shows the Arrhenius plot of the relaxation peak at different temperatures. Red line is the best linear fit.

electric modulus $M^*(\omega)$ is related to the Fourier transform of the time derivative of the electrical relaxation function, $\varphi(t)$, specifically, $M^*(\omega) = M_\infty\left[1 - \int_0^\infty \exp(-i\omega t)\frac{d\varphi}{dt}dt\right]$, where $M_\infty = \frac{1}{\varepsilon_\infty}$. Imaginary component ($M''$) of the complex electric modulus is shown in Fig. 3 as a function of frequency at various fixed temperatures. Signature of the asymmetric and significantly broad relaxation peak is observed from the frequency-dependent dielectric modulus as shown in Fig. 3. Interestingly, the width of the relaxation peaks decreases (from ~2.2 to ~1.8 decades) with an increase in temperature from 135 to 175 K. This value is considerably larger than the full width at half maximum (~1.14 decades) in ideal non-interacting dipolar relaxation described by the Debye relaxation function. Again, the relaxation peak frequency (f_p) is found to follow thermally activated Arrhenius behavior as shown in the inset of Fig. 3 which provides an estimation of the activation energy ~0.20 eV, close to the earlier mentioned estimated value.

The measured temperature-dependent dielectric permittivity at various fixed frequencies is shown in Fig. 4. In this measurement, the sample is first cooled to 80 K, and the dielectric permittivity was measured with increasing temperature. The thermally activated dielectric relaxation with temperature is shown by the arrow in Fig. 4. For all the measured frequencies, the dielectric constant drops to a very low value ~15 around liquid nitrogen temperature. Above and around room temperature, the dielectric permittivity shows a large value ~10^3 and is relatively less sensitive to temperature. As the frequency is increased, the relaxation temperature also increases obeying the thermally activated dielectric relaxation. Frequency variation of the loss tangent showed the characteristic loss peak (Fig. 4(b)) which is also

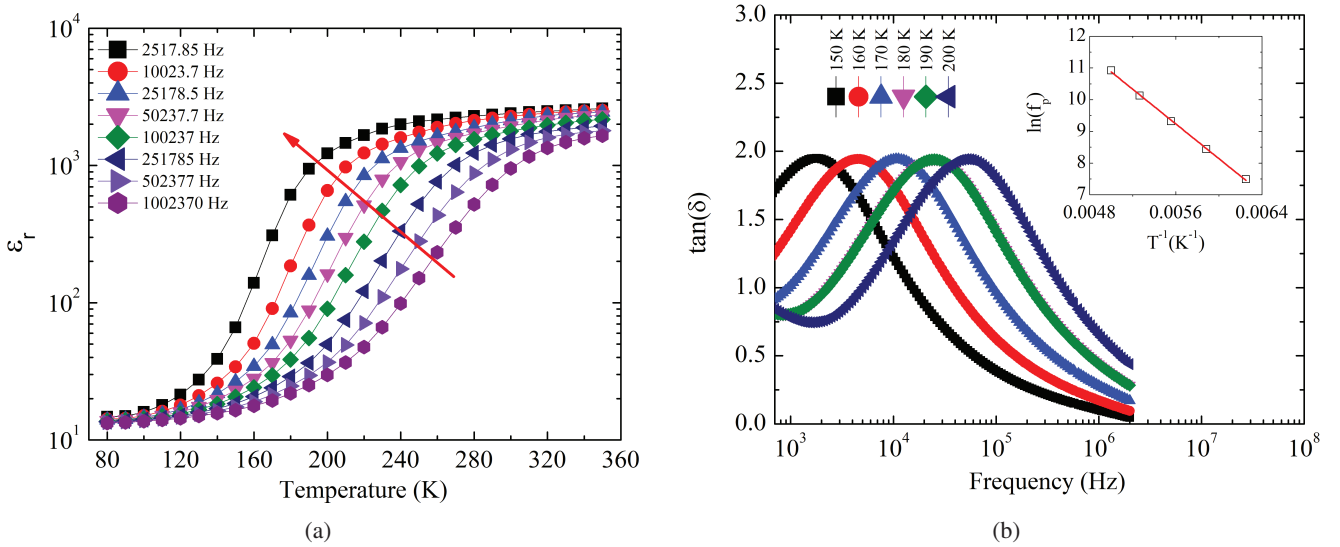

(a) (b)

Fig. 4. (Color online) (a) Temperature variation of relative dielectric permittivity for different frequencies. Thermally activated relaxation is marked by the arrow in the figure. (b) Thermal variation of loss tangent at selected frequencies. Inset of (b) is the Arrhenius plot of relaxation peak frequency observed in figure (b). Red line is the best linear fit.

thermally activated with an estimated activation energy ~0.21 eV. For the Eu_2CoMnO_6 compound with two different transition metal (Co and Mn) ions, a virtual hopping of charges between two dissimilar metal ions generates hopping polarization which gives rise to the observed dielectric relaxation. A similar dielectric relaxation due to hopping polarization was also observed in the closely related double perovskite La_2NiMnO_6.[10]

3.3. *AC conductivity and scaling*

AC conductivity (σ_{ac}) measurements provide considerable insight into the nature of conduction in disordered solids.[23] The conductivity spectra are shown in Figs. 5(a) and 5(b) for the low- and high-temperature regions, respectively. Figures 5(a) and 5(b) can be clearly divided into two separate regions. A plateau is noticed in the low-frequency side. For higher frequencies, on the other hand, a gradual dispersion sets in and indicates a power law (~f^n, n is constant) type dependence. Significant temperature dependence of conductivity is noticed in the low-frequency region in comparison to that in the high-frequency domain. The overall feature of the conductivity spectra appears to follow the empirical universal power law[23] behavior described by

$$\sigma_{ac}(f) = \sigma_0 + Af^n, \tag{2}$$

where $\sigma_{ac}(f)$ represents the frequency-dependent AC conductivity, σ_0 is the limiting value of AC conductivity when $f \to 0$,

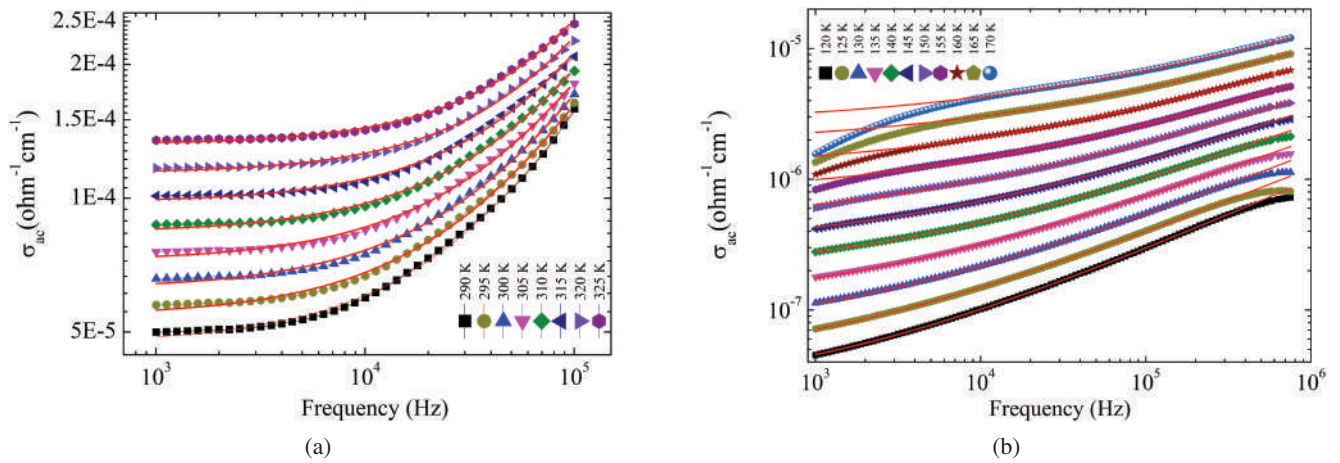

(a) (b)

Fig. 5. (Color online) AC conductivities as a function of frequency at different fixed temperatures are shown in figure (a) and in figure (b) for the high- and low-temperature regions, respectively. Red solid lines are the best fit to Eq. (2).

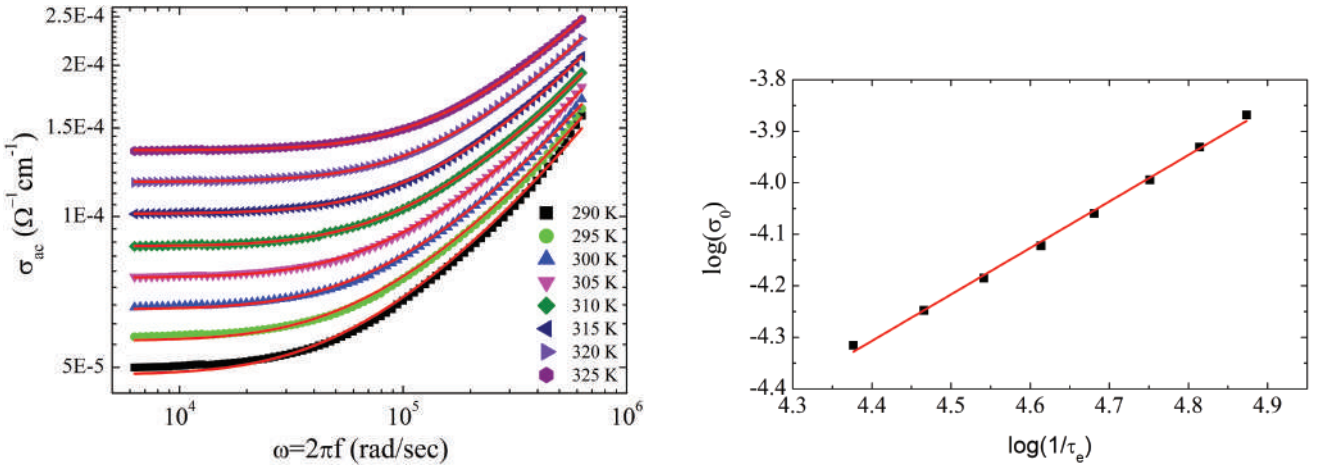

Fig. 6. (Color online) (a) Frequency variation of AC conductivity data fitted to Eq. (3) shown by red continuous line. (b) The fitting parameters τ_e and σ_0 of Eq. (3) are plotted to show the Barton–Nakajima–Namikawa (BNN) relation.

and A and n are two constants related to the strength of polarizability of the medium and interaction of mobile ions and lattices, respectively. The characteristic feature of the charge transport in many of the disordered semiconducting oxides and glassy materials usually obeys Eq. (2), referred to as the universal dynamic response (UDR).[23] Though a reasonable fitting is achieved with Eq. (2), it is important to mention that the exponent parameter n markedly differs in high and low temperatures. As mentioned earlier, the constant n is related to the interaction of the mobile ions and lattice, so this changing interaction with temperature may be responsible for the temperature dependence in n. The estimated exponent $n = 0.99$ at 325 K is found to monotonically decrease to 0.85 at 290 K. The frequency exponent n also decreases with temperature and lies between 0.6 and 0.4 in the temperature range (120–170 K) as seen in Fig. 5(b).

It is to be noted that Eq. (2) was derived based on the empirical description of σ_{ac} reportedly applied for a wide range of compounds. The σ_{ac} data were also analyzed in the light of the macroscopic theoretical model proposed by Dyre[24,25] where conductivity can be expressed by the relation

$$\sigma_{ac}(\omega) = \frac{\sigma_0 \omega \tau_e \arctan(\omega \tau_e)}{\frac{1}{4}\ln^2(1+\omega^2\tau_e^2) + (\arctan(\omega\tau_e))^2}. \quad (3)$$

Here $\sigma_{ac}(\omega)$ is the (angular) frequency dependent real part of the complex AC conductivity, σ_0 is the limiting value of σ_{ac} when $f \to 0$, ω is the angular frequency and τ_e is the relaxation time. Equation (3) provides a basis to analyze conduction phenomena on a theoretical level which is based on the random free energy barrier model developed by Dyre.[24] Within the CTRW approximation, conduction is assumed to take place by the hopping of charge carriers in a spatially randomly varying energy landscape. Interestingly, reasonable fitting with Eq. (3) is also observed in the high-temperature region (red continuous line in Fig. 6(a)). However, the said

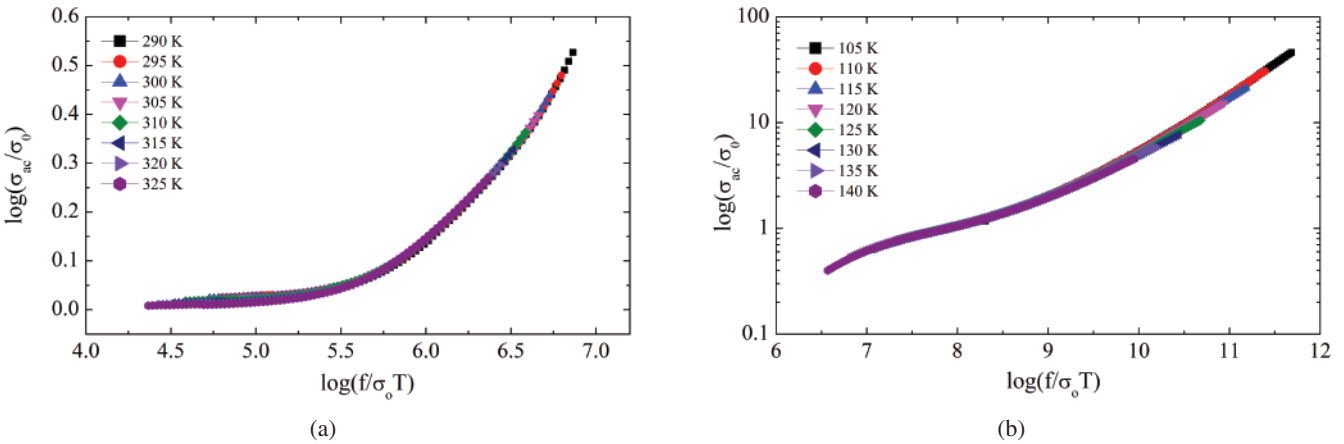

Fig. 7. (Color online) Scaling of AC conductivity in high- and low-temperature regions is presented in figures (a) and (b), respectively.

macroscopic theoretical CTRW model (Eq. (3)) failed to fit the corresponding low-temperature (not shown) conductivity data. Thus, it is apparent that two different microscopic conduction mechanisms are operative at high- and low-temperature regions. It is noteworthy to mention that the fitting parameters τ_e and σ_0 are in good agreement with those of the Barton–Nakajima–Namikawa (BNN) relation[26] which is evident from the straight-line feature of the curve shown in Fig. 6(b).

Scaling is widely used to investigate the possible underlying common physical mechanisms for conduction.[27,28] Hence, the scaling characteristics of the σ_{ac} spectra are also examined for the present sample. The result presented in Figs. 7(a) and 7(b) indicates that the conductivity spectra can be scaled to a master curve in both the high- and low-temperature regions. The zero frequency limiting value of AC conductivity σ_0 was taken as the scaling parameter for σ_{ac}. The products of σ_0 and T were used for the scaling parameters for the frequency scale. The choice of scaling parameter is identical to that of canonical scaling.[28] Similar scaling characteristics were also reported in disordered semiconductor type materials.[29,30] The estimated scaling parameters suggested that the shape of the relaxations' function was not dependent separately on the frequency and temperature, but together as a product of frequency and temperature. Though low-temperature data could not be reproduced by Eq. (3), the scaling properties retained in the conductivity spectra (with the same choice of scaling parameters similar to the high-temperature side) as shown in Fig. 7(b). Although the time scale of the relaxation varies with temperature, it is apparent that the spectral features of the relaxation functions contribute at all temperatures to preserve the scaling features.

4. Conclusion

We have synthesized the single phase double perovskite Eu_2CoMnO_6 and compared the structural properties with another closely related isostructural compound Eu_2NiMnO_6 which revealed the interesting role of bond lengths, bond angles, polyhedral shape and volume on the physical properties of Eu_2CoMnO_6. Quite a high value of relative dielectric permittivity ~10^3 with weak temperature dependent behavior (for frequencies below 100 kHz) was detected around ambient temperatures. The observed dielectric relaxation was attributed to the hopping polarization between two different Co and Mn cationic potential wells in a disordered cationic environment. The nature of dielectric relaxation is successfully explained with the HN type relaxation function revealing the important role of anti-site disorder in the dielectric properties. Asymmetric and broadened dielectric relaxations in both temperature and frequency variations indicated the prospective role of anti-site disorder developed during the growth of the double perovskite Eu_2CoMnO_6. The AC conductivity qualitatively followed empirical UDR governed by the Jonscher power law. However, it is noted that the macroscopic CTRW approximation model proposed by Dyre is applicable only in the high-temperature region. Hence, it can be concluded that some different or additional microscopic conduction mechanism influences the conductivity behavior in the low-temperature region. Finally, success to scale different data sets to collapse all to one common master curve indicates that the underlying conduction mechanism can be separated into a common physical mechanism modified by thermodynamic scales only.

Acknowledgments

The authors gratefully acknowledge the central and other measurement facilities provided by the Solid State Physics Department, Indian Association for the Cultivation of Science (IACS), Kolkata, India.

References

[1]H. R. Fuh, Y. P. Liu, Z. R. Xiao and Y. K. Wang, New type of ferromagnetic insulator: Double perovskite La_2NiMO_6 (M=Mn, Tc, Re, Ti, Zr, and Hf), *J. Magn. Magn. Mater*. **357**, 7 (2014).

[2]Y. K. Wakabayashi, Y. Krockenberger, N. Tsujimoto, T. Boykin, S. Tsuneyuki, Y. Taniyasu and H. Yamamoto, Ferromagnetism above 1000 K in a highly cation-ordered double-perovskite insulator Sr_3OsO_6, *Nat. Commun*. **10**, 535 (2019).

[3]J. Frantti, Y. Fujioka, C. Rouleau, A. Steffen, A. Puretzky, N. Lavrik, I. N. Ivanov and H. M. Meyer, In quest of a ferromagnetic insulator: Structure-controlled magnetism in Mg–Ti–O thin films, *J. Phys. Chem. C* **123**, 32, 19970 (2019).

[4]K. I. Kobayashi, T. Kimura, H. Sawada, K. Terakura and Y. Tokura, Room-temperature magnetoresistance in an oxide material with an ordered double-perovskite structure, *Nature* **395**, 677 (1998).

[5]H. Kato, T. Okuda, Y. Okimoto and Y. Tomioka, Metallic ordered double-perovskite Sr_2CrReO_6 with maximum Curie temperature of 635 K, *Appl. Phys. Lett*. **81**, 328 (2002).

[6]M. K. Kim, J. Y. Moon, S. H. Oh, D. G. Oh, Y. J. Choi and N. Lee, Strong magnetoelectric coupling in mixed ferrimagnetic-multiferroic phases of a double perovskite, *Sci. Rep*. **9**, 5456 (2019).

[7]M. P. Singha, K. D. Truong, S. Jandl and P. Fournier, Multiferroic double perovskites: Opportunities, issues, and challenges, *J. Appl. Phys*. **107**, 09D917 (2010).

[8]S. Yamada, N. Abe, H. Sagayama, K. Ogawa, T. Yamagami and T. Arima, Room-temperature low-field colossal magnetoresistance in double-perovskite manganite, *Phys. Rev. Lett*. **123**, 126602 (2019).

[9]M. G. Masud, A. Ghosh, J. Sannigrahi and B. K. Chaudhuri, Observation of relaxor ferroelectricity and multiferroic behaviour in nanoparticles of the ferromagnetic semiconductor La_2NiMnO_6, *J. Phys. Condens. Matter*. **24**, 295902 (2010).

[10]D. Choudhury, P. Mandal, R. Mathieu, A. Hazarika, S. Rajan, A. Sundaresan, U. V. Waghmare, R. Knut, O. Karis, P. Nordblad and D. D. Sarma, Near-room-temperature colossal magnetodielectricity and multiglass properties in partially disordered La_2NiMnO_6, *Phys. Rev. Lett*. **108**, 127201 (2012).

[11]M. Ullah, S. A. Khan, G. Murtaza, R. K. NaeemUllah and S. B. Omran, Electronic, thermoelectric and magnetic properties of La_2NiMnO_6 and La_2CoMnO_6, *J. Magn. Magn. Mater*. **377**, 197 (2015).

[12]R. Egoavil, S. Hühn, M. Jungbauer, N. Gauquelin, A. Béché, G. Van Tendeloo, J. Verbeecka and V. Moshnyaga, Phase problem in the B-site ordering of La_2CoMnO_6: Impact on structure and magnetism, *Nanoscale* **7**, 9835 (2015).

[13]C. Zhang, W. Zhu, L. Yuan and H. Yuan, B-site ordering, magnetic and dielectric properties of hydrothermally synthesized Lu_2NiMnO_6, *J. Alloys Compd*. **744**, 395 (2018).
[14]Y. Q. Lin, S. Y. Wu and X. M. Chen, Effects of ordering domain structure on dielectric properties of double perovskite La_2NiMnO_6, *J. Adv. Dielectr*. **01**, 319 (2011)
[15]A. K. Singh, S. Chauhan, S. K. Srivastava and R. Chandra, Influence of anti-site disorders on the magnetic properties of double perovskite Nd_2NiMnO_6, *Solid State Commun*. **242**, 74 (2016).
[16]Y. Zhang, H. Li, D. Guo, L. Hou, X. Li, Z. Ren and G. Wilde, Cryogenic magnetic properties and magnetocaloric performance in double perovskite Pr_2NiMnO_6 and Pr_2CoMnO_6 compounds, *Ceram. Int*. **44**, 17 (2018).
[17]M. G. Masud, H. Sakata, A. K. Biswal, P. N. Vishwakarma and B. K. Chaudhuri, Structural, ac conductivity scaling and magneto-dielectric behaviour of a partially disordered insulating ferromagnetic double perovskite Eu_2NiMnO_6, *J. Phys. D. Appl. Phys.* **48**, 375504 (2015).
[18]M. Alam, P. Singh, K. Anand, A. Pal, S. Ghosh, A. K. Ghosh, R. K Singh, A. G. Joshi and S. Chatterjee, Extraordinary magnetic properties of double perovskite Eu_2CoMnO_6 wide band gap semiconductor, *J. Phys. Condens. Matter* **32**, 365802 (2020).
[19]J. Krishnamurthy and A. Venimadhav, Magnetic field-induced metamagnetic, magnetocaloric and pyrocurrent behaviors of Eu_2CoMnO_6, *J. Magn. Magn. Mater*. **500**, 166387 (2020).
[20]R. Rai, M. A. Valente, A. K. Shukla, S. Sharma and A. L. Kholkin, Dielectric and magnetic properties of Ba-, La- and Pb-doped $Bi_{0.8}Gd_{0.1}M_{0.1}Fe_{0.9}Ti_{0.1}O_3$ perovskite ceramics, *J. Adv. Dielectr*. **04**, 1450010 (2014).
[21]K. C. Kao, *Dielectric Phenomena in Solids* (Elsevier Academic Press, London, 2004); R. M. Hill and L. A. Dissado, Debye and non-Debye relaxation, *J. Phys. C. Solid State Phys*. **18**, 3829 (1985).
[22]S. Havriliak and S. Negami, A complex plane representation of dielectric and mechanical relaxation processes in some polymers, *Polymer* **8**, 161 (1967).
[23]A. K. Jonscher, *Universal Relaxation Law* (Chelsea Dielectrics Press, London, 1996).
[24]J. C. Dyre, The random free-energy barrier model for ac conduction in disordered solids, *J. Appl. Phys*. **64**, 2456 (1988).
[25]E. Montroll and G. H. Weiss, Random walks on lattices. II, *J. Math. Phys*. **6**, 167 (1965).
[26]J. C. Dyre and T. B. Schroder, Universality of ac conduction in disordered solids, *Rev. Mod. Phys*. **72**, 873 (2000).
[27]D. L. Sidebottom, Universal approach for scaling the ac conductivity in ionic glasses, *Phys. Rev. Lett*. **82**, 18 (1999).
[28]D. L. Sidebottom, Understanding ion motion in disordered solids from impedance spectroscopy scaling, *Rev. Mod. Phys*. **81**, 3 (2009).
[29]A. R. Kulkarni, P. Lunkenheimer and A. Loidl, Scaling behaviour in the frequency dependent conductivity of mixed alkali glasses, *Solid State Ion*. **112**, 69 (1998).
[30]M. T. Connor, S. Roy, T. A. Ezquerra and F. J. Baltá Calleja, Broadband ac conductivity of conductor-polymer composites, *Phys. Rev. B* **57**, 2286 (1998).